Additive Manufacturing 32 (2020) 101041

Contents lists available at ScienceDirect

Additive Manufacturing

journal homepage: www.elsevier.com/locate/addma

Full Length Article

Prediction of anisotropic mechanical properties for lattice structures

Maxwell Munford, Umar Hossain, Shaaz Ghouse, Jonathan R.T. Jeffers*

Department of Mechanical Engineering, Imperial College London, South Kensington, London SW7 2AZ, United Kingdom

ARTICLE INFO

Keywords:
Additive manufacturing
Lattice
Titanium
Nylon
Anisotropic
Fabric
Density

ABSTRACT

Additive manufacturing methods present opportunities for structures to have tailored mechanical anisotropy by integrating controlled lattice structures into their design. The ability to predict anisotropic mechanical properties of such lattice structures would help tailor anisotropy and ensure adequate off-axis strength at an early stage in the design process. A method is described for the development of a model to predict apparent modulus and strength based on structure density and fabric, taken from CAD data. The model utilises a tensorial form of well-founded power-law relationships for these variables and is fit to mechanical test data for properties in the principal directions of manufactured titanium stochastic lattices and nylon rhombic dodecahedron structures. The results are validated against mechanical testing across at least 7 additional off-axis directions. For stochastic structures, apparent modulus is predicted in 10 directions with a mean error of 13% and strength predicted with a mean error of 10%. For rhombic dodecahedron structures apparent modulus and strength are predicted in 15 directions with mean errors of 4.2% and 5.1% respectively. This model is the first to predict the anisotropic apparent modulus and strength of structures based on lattice density and fabric tensors and will be highly useful in the mechanical design of lattice structures.

1. Introduction

Development of additive manufacturing (AM) methods has enabled fine control of mechanical and morphological properties when producing porous lattice structures [1–3]. In this way the internal architecture of an additively manufactured component can be assessed and optimised for specific mechanical performance, such as custom modulus and strength properties, porosity and novel surface features [4–6]. The use of lattice structures has been widely expanded across industries such as orthopaedics, aeronautics and defence due to the efficiency of mass distribution in the structure [7–10].

Orthopaedic implants are traditionally manufactured from materials with bulk modulus significantly greater than that of bone, thus changing the load transfer in bone from the physiological norm [11]. AM lattice structures are a viable route to achieve implants which match the mechanical properties of bone and thus maintain physiological load transfer [12,13]. In aerospace applications, lattice structures manufactured from carbon-fibre-reinforced plastics have been commonly used for interstage structures in launch vessels due to high axial compressive strength-to-weight ratio [9]. Military unmanned aerial vehicles have been developed utilising optimised lattice structures so that components can have optimal elastic modulus and natural frequencies [10,14]. In all cases, components would benefit from either being isotropic or having designed mechanical anisotropy, potentially dissimilar to their repeating unit cell. AM enables such components to be manufactured, but understanding and predicting the anisotropy is a new requirement in the design stage of lattice structures.

Examples of existing methods for measuring the anisotropy of lattice structures include mechanical testing and finite element (FE) methods. Mechanical testing is ideal and some previous work, such as that presented by Weissman et al. [15] attempts this in multiple directions. Although this method is ideal, it can be difficult to determine repeated measurements and does not account for any hidden peaks or troughs which may be present in some structures, as explained by Sallica-Leva et al. and Challis et al. [3,16]. In particular, repeating cell structures often have hidden axis of high modulus or strength. FE methods can be easier to set up and control and allow testing in different directions. Such methods have been shown by Xu et al. and Stanković et al. [17,18]. However, results are dependent on FE model parameters and should be validated against mechanical testing, examples of uniaxial and multiaxial validation are shown by Challis et al. and Takezawa et al. respectively [3,19]. Predictions of mechanical properties in porous structures, most notably bone, based on isotropic power laws between apparent modulus and density are well founded [20]. Similar isotropic or uniaxial power law models have been used to describe the mechanical behaviour of porous structures, manufactured by AM

* Corresponding author.
E-mail address: j.jeffers@imperial.ac.uk (J.R.T. Jeffers).

https://doi.org/10.1016/j.addma.2020.101041
Received 11 September 2019; Received in revised form 6 December 2019; Accepted 4 January 2020
Available online 23 January 2020

methods or otherwise. Some more recent literature on this topic has sought to incorporate the concept of fabric into models for bone properties, however, these usually require high resolution micro-CT data [21–23]. These methods rely on an initial set of mechanical data to define model parameters. Fabric is a statistical measure of material directionality and helps to model a lattice or trabecular structured material as a bulk material with directional bias in properties [24]. Fabric-based methods have not yet been applied to the analysis of PBF-printed lattice structures.

The aim of the paper is to develop a method for predicting the anisotropy in mechanical properties of a stochastic lattice structure, based on CAD data. The model predicts anisotropic apparent modulus and strength in terms of density (ρ), fabric (**M**) and fabric eigen values (m), inspired by previous methods of measuring bone anisotropy. This method would be highly useful to predict the apparent modulus and anisotropy of lattice structures in order to tailor anisotropy and ensure adequate off-axis strength at an early stage in the design process.

2. Material and methods

2.1. Specimen design and manufacture

Two lattice structures were investigated, one stochastic and one repeating cell rhombic dodecahedron. Specimens for each lattice type were designed and manufactured as follows.

2.1.1. Stochastic structure

The stochastic structure was created by populating a volume with pseudo-random points using a Poisson disk algorithm, maintaining a specific minimum proximity. These points were then joined with lines to achieve a certain connectivity. This method, which uses Rhinoceros 5.0 and Grasshopper (Robert McNeel & Associates) is described by Ghouse et al. [25]. The density of the structure was 4.06 struts/mm^3 and with an average connectivity at each node of 5.80. Lines at an angle of less than 30° inclination to the x-y plane were culled to ensure good printability for AM manufacturing.

A points based exposure strategy, developed by Betatype Ltd, was used to melt the required cross section of each micro-strut [25]. Slice data (build files) were generated at 50 µm layer thickness using Material Engine (Betatype Ltd).

All specimens were printed using a Renishaw AM250 PBF additive manufacturing system (Renishaw, Wooton Under Edge, UK). Titanium (Ti6Al4V ELI) spherical powder of particle size range 10–45 µm was used, supplied by LPW Technology (Widnes, UK). The build chamber was vacuumed to -960 mbar and then back filled with 99.995% pure Argon to 10 mbar with an O content of ∼0.1%. Laser power was constant at 50 W whilst exposure times varied from 600 to 1700 µs to maintain a constant strut thickness regardless of build angle.

Specimens were removed from the build-plate by electro-discharge machining, ensuring that the wire path preserved the intended part geometry, then cleaned using ultrasonic bath and air jet. Each specimen was individually measured thrice in each dimension using Vernier callipers, and dry weighed thrice at normal atmospheric conditions. The relative density was then calculated by dividing the specimen weight by the bulk weight of the metal that corresponds to the specimen macro volume, assuming a density of 4.43 g/cm^3 for Ti6Al4V.

2.1.2. Rhombic dodecahedron structure

The rhombic dodecahedron structure was created using a lattice plugin for Rhinoceros 5.0 and Grasshopper. No lines were culled in this design. The rhombic dodecahedron specimens were 3D printed in medical grade Nylon (PA 2200) using an EOS P110 (EOS, Warwick, UK).

2.1.3. Structure orientation

For both the stochastic and rhombic dodecahedron structures, cuboid compression specimens were generated containing the structure aligned in different directions to the testing axis, as per the spherical coordinates in Table 1a and b. This allows testing of modulus and strength in multiple axes, where strength has been defined as the 1% offset yield stress. Fig. 1 illustrates how the spherical coordinates were used to determine specimen orientation and print direction. For the stochastic specimens, 5 specimens were tested per direction, with dimensions 10 × 10 × 12 mm and for the rhombic dodecahedron cell specimens, 2 specimens were tested per direction with dimensions 15 × 15 × 20.5 mm. All specimens conformed to ISO 13,314:2011 [26].

Table 1
Spherical coordinates of structure test directions for (a) stochastic specimens and (b) rhombic dodecahedron specimens.

a Direction	θ	φ
0	0	90
1	45	35
2	0	0
3	90	45
4	20	19
5	90	0
6	0	45
7	70	19
8	45	0
9	45	63

b Direction	θ	φ
0	0	0
1	30	0
2	45	0
3	60	0
4	30	30
5	30	45
6	30	60
7	45	30
8	45	45
9	45	60
10	60	30
11	60	45
12	60	60
13	90	0
14	0	90

2.2. Calculation of fabric tensors and fitting of predictive model

Directional data of the generated structure was extracted from the CAD model and used to determine a fabric moment tensor from a list of direction vectors based on mean intercept length (MIL) methods as follows [27].

A list of the vectors describing all of the struts in the CAD line files in Fig. 2a were exported from Rhino 6 into MATLAB [28]. The distribution of vectors shown in Fig. 2b illustrates how all struts below 30° inclination to the x-y plane have been removed. The fabric moment tensor ellipsoid representation in Fig. 2c has the expected characteristic hourglass shape of an orthotropic structure. The fabric tensor is a second order symmetric tensor with eigen values (λ_1, λ_2, λ_3) and eigen vectors ($\boldsymbol{\lambda}_1$, $\boldsymbol{\lambda}_2$, $\boldsymbol{\lambda}_3$) which describe the magnitude and direction of the structure principal directions indicated in Fig. 2c.

This process was repeated for the rhombic dodecahedron structure to yield a different symmetric second order fabric tensor to describe the distribution of material orientation in the rhombic dodecahedron lattice.

The predictive model for lattice apparent modulus was based on a tensorial form of Cowin's fabric-elasticity equations, similar to that described by Zysset-Curnier [22]. This model allowed conversion from

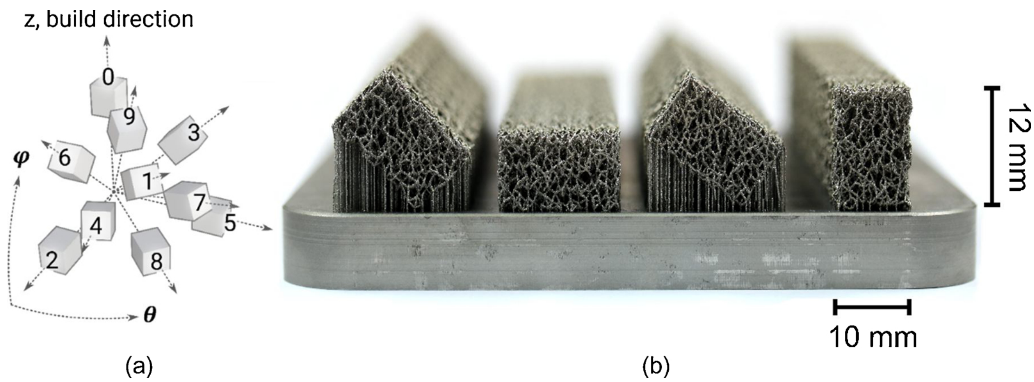

Fig. 1. (a) Stochastic specimen orientations for all 10 test directions based on spherical coordinates in Table 1a and (b) the corresponding printed specimens.

lattice density and fabric data to orthotropic elastic properties. This model builds upon the commonly used density-modulus power law relationship stated by Gibson and Ashby [29] ($\lambda\rho^k$) by introducing power terms which include the eigenvalues (*m(i)*). The use of a different power term for each fabric eigenvalue (*l(i)*) differentiates this model from similar models in literature.

$$\boldsymbol{S} = \sum_{i,j=1}^{i,j=3} \lambda(i,j)\rho^k m(i)^{l(i)} m(j)^{l(j)} |\boldsymbol{M}_i \otimes \boldsymbol{M}_j|^2 \tag{1}$$

Multivariate linear regression was performed to fit the data for density and fabric eigenvalues to the experimentally measured apparent modulus in the three orthogonal principal directions only (described in Section 2.3), to form the theoretical model described by Eq. 1 (see Table 2). In Eq. 1, k represents the exponent similar to that present in traditional power law models for porous structures [29], l represents the effects of the structure orientation given by the fabric eigenvalues and λ represents the transformation between the structural and mechanical properties. This was repeated to fit the density and fabric eigenvalues to the strength data. In this manner, orthotropic compliance and stress tensors were formed from the observed apparent modulus and strength along principal directions (Table 2) based on sample by sample values from all repeated measurements, not averaged mechanical data values. Low-high bounds of densities correlated to the respective bounds of apparent modulus and strength. To generate the parameters defining the model for apparent modulus, components of the orthotropic tensor were aligned in a vector $\boldsymbol{y}$. A log transformation was applied to the density, fabric eigenvalues, mechanical property values and regression coefficients to obtain a multiple linear regression model of the form $\boldsymbol{y} = \boldsymbol{X}\boldsymbol{c} + \boldsymbol{e}$, whereby $\boldsymbol{X}$ is a 10 x n matrix containing the density and fabric information for the model, **c** is a vector containing the constants which define Eq. 1 and **e** is the vector of the residuals. A complete form of this equation is given in the Appendix. This system of equations was then solved for the 10 model parameters contained in the vector **c** as per Eq. 2.

$$\boldsymbol{c} = \begin{bmatrix} ln(\lambda_{1,1}) & In(\lambda_{2,2}) & In(\lambda_{3,3}) & In(\lambda_{1,2}) & In(\lambda_{1,3}) & In(\lambda_{2,3}) & k & l_1 & l_2 & l_3 \end{bmatrix}' \tag{2}$$

This process was repeated with the elements of vector $\boldsymbol{y}$ replaced by components of the orthotropic stress tensor to determine coefficients for the strength model. The variables in **c** define Eq. 1 to yield anisotropic tensors for apparent modulus and strength in terms of the known density ρ, fabric eigenvalues m_i and fabric eigenvector dyadic $\boldsymbol{M}_i$. The fabric dyadics are defined by Eq. 3.

$$\boldsymbol{M}_i = \lambda_i \otimes \lambda_i \tag{3}$$

The apparent density could not be accurately recorded for the nylon specimens due to the un-removable presence of semi-sintered and loose powder from the manufacturing process deep inside the structure. The density term (ρ) in Eq. 1 was therefore neglected and k set to 0 so that the models for predicting apparent modulus and strength of nylon lattice structures were based on fabric only, found from CAD data. The parameters defining models for nylon lattices were therefore valid only

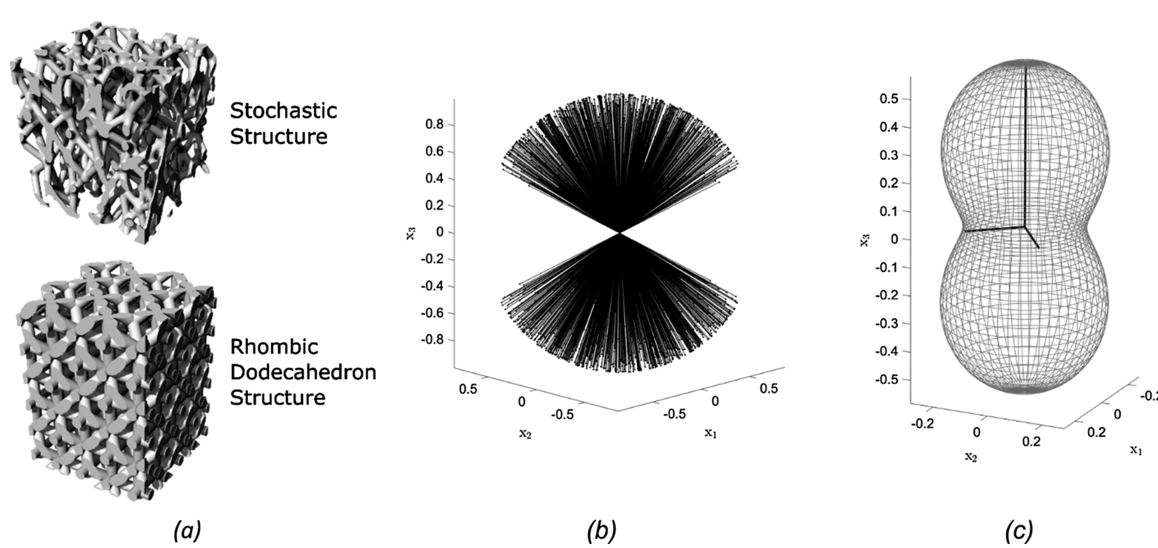

Fig. 2. (a) CAD line structure file for the stochastic and rhombic dodecahedron structures built as in Section 2.1. (b) Directional data for the 2155 line vectors comprising the stochastic structure in (a). (c) Ellipsoid representation (grey) and weighted principal directions for the fabric moment tensor for the stochastic structure in (a).

Table 2
Summary of specimen build direction, density, fabric and mechanically tested apparent modulus and peak strength data for the orthogonal axis stochastic and rhombic dodecahedron lattice structures.

	Build Direction	n	Apparent Density [g/cm^3]	$\boldsymbol{M}$	Apparent Modulus [MPa]	Peak Strength [MPa]
Titanium	0	5	697.6 – 704.1	$\begin{bmatrix} 0.2097 & 0.0043 & 0.0025 \\ 0.0043 & 0.2079 & 0.0038 \\ 0.0025 & 0.0038 & 0.5824 \end{bmatrix}$	2920 – 2980	37.72 – 39.47
	2	5	693.6 – 700.1		740 – 790	15.92 – 16.65
	5	5	672.0 – 685.4		610 – 670	14.05 – 14.80
	0	2	Not Applicable	$\begin{bmatrix} 0.3632 & 0.0028 & 0.0002 \\ 0.0028 & 0.3646 & 0.0006 \\ 0.002 & 0.0006 & 0.2722 \end{bmatrix}$	159 - 160	5.47 – 5.51
	14	2			99.6 – 121	3.94 – 4.24
	15	2			99.6 - 121	3.94 – 4.24

for the lattice density tested here.

2.3. Mechanical measurement of anisotropic properties

A materials testing machine (Instron 8872) with a 10 kN load cell was used to perform quasi-static compression testing at an extension rate of 2 mm/min, which corresponds to initial strain rates of 2.7×10^{-3} s^{-1} and 1.6×10^{-3} s^{-1} for the stochastic and rhombic dodecahedron specimens respectively. These values comply with standard limits of between 10^{-3} s^{-1} and 10^{-2} s^{-1} [30].

Displacement was measured using LVDTs to reduce any compliance effects from the test apparatus. A sampling rate of 30 Hz was used. The platens of the machine were lubricated to reduce any frictional effects. Stress-strain curves were obtained using the macro dimensions of each specimen.

The loading regime includes a hysteresis loop to account for localised plasticity within the porous structure during initial loading. This was carried out from 70% of the yield stress (σ_{70}), to 20% of the yield stress (σ_{20}) and then the specimen is fully compressed to a high strain [30]. The elastic moduli were then calculated using a linear regression analysis of the hysteresis loop. A preliminary specimen was compressed to 50% strain at 2 mm/min to find the required reference stresses. Fig. 3 illustrates how the apparent modulus, yield and peak strength were determined for the Titanium stochastic structures, where yield stress was taken as the 1% offset stress. Testing of preliminary specimens suggested that the peak and yield stress were almost identical for these specimens, peak stress was therefore measured as an indicator of lattice strength. For the nylon rhombic dodecahedron specimens, the 1% offset stress was used as an indicator of strength.

For each structure type, all structures were generated from the same lattice CAD file so therefore had the same fabric tensor, as indicated in Table 2. Eigenvalue decomposition for the titanium stochastic structures yields the equivalent Eigenvalues (λ) and Eigenvectors ($\boldsymbol{\lambda}$) for this tensor as:

$$\begin{bmatrix} \lambda_1 \\ \lambda_2 \\ \lambda_3 \end{bmatrix} = \begin{bmatrix} 0.2044 \\ 0.2131 \\ 0.5825 \end{bmatrix} \text{and} [\boldsymbol{\lambda}_1 \quad \boldsymbol{\lambda}_2 \quad \boldsymbol{\lambda}_3] = \begin{bmatrix} 0.6313 & 0.7755 & 0.0069 \\ -0.7755 & 0.6313 & 0.0102 \\ 0.0035 & -0.0118 & 0.9999 \end{bmatrix}$$

Similarly, eigenvalue decomposition for the nylon rhombic dodecahedron structures yields the equivalent Eigenvalues (λ) and Eigenvectors ($\boldsymbol{\lambda}$) for this tensor as:

$$\begin{bmatrix} \lambda_1 \\ \lambda_2 \\ \lambda_3 \end{bmatrix} = \begin{bmatrix} 0.2722 \\ 0.3610 \\ 0.3668 \end{bmatrix} \text{and} [\boldsymbol{\lambda}_1 \quad \boldsymbol{\lambda}_2 \quad \boldsymbol{\lambda}_3] = \begin{bmatrix} 0.0018 & -0.7908 & -0.6121 \\ 0.0066 & 0.6121 & -0.7908 \\ 1 & -0.0026 & 0.0063 \end{bmatrix}$$

3. Results

The regression methods described in Section 2.2 define the model parameters λ, l and k for prediction of apparent modulus and peak strength for both lattice types as in Table 3.

3.1. Stochastic lattice results

The model for the titanium stochastic lattice predicted the apparent modulus of the structure across all 10 orientations (Fig. 4a). A linear relationship between the measured and predicted values was found ($R^2 = 0.969$), with a 0.2 GPa offset indicating the model slightly overpredicted the apparent modulus of the off-axis directions. The predicted and measured anisotropy both generated the hour-glass shape for 3 dimensional modulus (Fig. 4b). The closest prediction was for orthogonal directions 0, 2 and 5 which was expected as the experimental values from these directions were used to define the model. The model overpredicted modulus in directions 1, 3, 6 and 9 by 16–23%. In directions 4, 7 and 8 the model over predicted by between 12 and 16%.

The model predicted the peak strength of the structure across all 10 orientations (Fig. 5a). A linear relationship between the measured and predicted values was found ($R^2 = 0.943$), with a 2.9 MPa offset

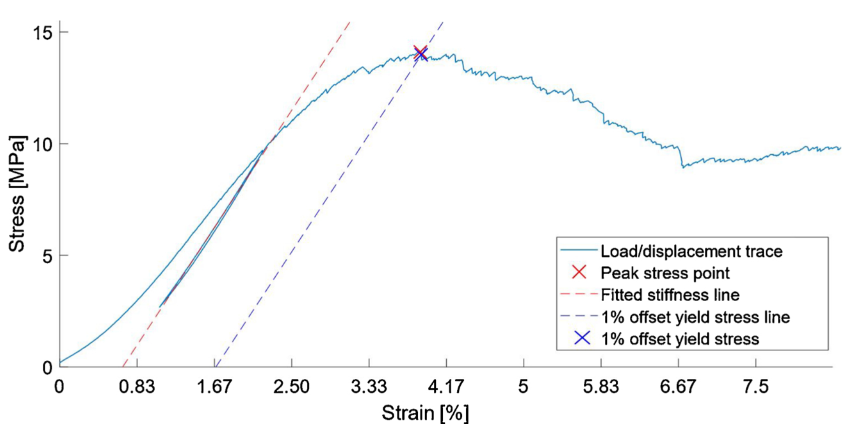

Fig. 3. Typical load-displacement curve for a stochastic titanium structure with mechanical properties determined as apparent modulus = 0.66 GPa, peak stress = 14.7 MPa and 1% offset yield stress = 14.51 MPa.

Table 3
Parameters defining the model in Eq. 1 for predicting both apparent modulus and strength of the stochastic lattice and the rhombic dodecahedron lattice.

Lattice	Parameter	λ	l	k
Stochastic	Apparent Modulus	$\begin{bmatrix} 1 & 0.11 & 0.42 \\ 0.11 & 1 & 0.52 \\ 0.42 & 0.52 & 1 \end{bmatrix}$	$\begin{bmatrix} 1.38 \\ 1.46 \\ 2.82 \end{bmatrix}$	1.68
	Strength	$\begin{bmatrix} 1 & 0.11 & 1.85 \\ 0.11 & 1 & 2.23 \\ 1.85 & 2.23 & 1 \end{bmatrix}$	$\begin{bmatrix} 2.79 \\ 2.88 \\ 7.40 \end{bmatrix}$	1.78
Rhombic Dodecahedron	Apparent Modulus	$\begin{bmatrix} 1 & 0.07 & 0.08 \\ 0.07 & 1 & 0.12 \\ 0.08 & 0.12 & 1 \end{bmatrix}$	$\begin{bmatrix} -1.81 \\ -2.31 \\ -2.53 \end{bmatrix}$	0
	Strength	$\begin{bmatrix} 1 & 0.07 & 0.09 \\ 0.07 & 1 & 0.12 \\ 0.09 & 0.12 & 1 \end{bmatrix}$	$\begin{bmatrix} -0.54 \\ -0.69 \\ -0.85 \end{bmatrix}$	0

indicating the model also slightly overpredicted the peak strength of the off-axis directions. The predicted and measured anisotropy both generated the hour-glass shape for 3 dimensional modulus (Fig. 5b). As with the apparent modulus model, the closest prediction was for orthogonal directions 0, 2 and 5 which was expected as the experimental values from these directions were used to define the model. The model overpredicted strength in directions 1, 3, 6 and 9 by 14–18%. In directions 4, 7 and 8 the model over predicted by between 8 and 16%.

The predictive model provided a close apparent modulus-strength relationship to the measured relationship (Fig. 6). For a given modulus, the model slightly over predicted the strength, but by less than 8% across the 0.5–3 GPa test range. Both predicted and measured relationships had a power relationship with $R^2 = 0.99$.

3.2. Rhombic dodecahedron lattice results

The model for the nylon rhombic dodecahedron lattice predicted the apparent modulus of the structure across all 15 orientations (Fig. 7). A linear relationship between the measured and predicted values was found ($R^2 = 0.86$), with a 21.3 MPa offset indicating the model slightly overpredicted the apparent modulus of the off-axis directions. The predicted and measured anisotropy both generated the ellipsoid for 3 dimensional modulus (Fig. 7b). The closest prediction was for orthogonal directions 0, 13 and 14 which was expected as the experimental values from these directions were used to define the model. On average, the model underpredicted apparent modulus in directions which were inclined 30 degrees to the horizontal (directions 1, 4, 5 and 6) with a mean absolute error of 7%. For directions 2, 7, 8 and 9, which are inclined at 45 degrees to the horizontal, the model consistently underpredicted values to within 8.9%. Across directions 3, 10, 12 and 13, which are 60 degrees to the horizontal, the model predicted apparent modulus values to within 7.6%.

The model predicted the strength of the structure across all 15 orientations (Fig. 8a). A linear relationship between the measured and predicted values was found ($R^2 = 0.840$), with a -0.13 MPa offset indicating the model also slightly underpredicted the strength of the off-axis directions. The predicted and measured anisotropy both generated the ellipsoid shape for 3 dimensional modulus (Fig. 8b). As with the apparent modulus model, the closest prediction was for orthogonal directions 0, 13 and 14, which was expected as the experimental values from these directions were used to define the model. The model underpredicted peak stress across all directions which were inclined 30 degrees to the horizontal (directions 1, 4, 5 and 6) with a mean absolute error of 8.8%. For directions 2, 7, 8 and 9, which are inclined at 45 degrees to the horizontal, the model predicted values to within 5%. Across directions 3, 10, 12 and 13, which are 60 degrees to the horizontal, the model predicted apparent modulus values to within 5.9% absolute error.

The predictive models for nylon rhombic dodecahedron structures provided a close apparent modulus-strength relationship to the measured relationship (Fig. 9). For a given modulus, the model slightly underpredicted the strength for lower moduli and overpredicted strength for larger moduli values, always within 10.2% across the 0.1 – 0.16 GPa test range. Both predicted and measured relationships had a power relationship with $R^2 = 0.99$.

4. Discussion

This study demonstrates that the off-axis apparent modulus and strength of lattice structures can be predicted with good accuracy using fabric/elasticity equations. This is a highly useful tool, enabling the strength and anisotropy of lattices to be determined while the component is at an early stage in the design process. It does not eliminate the need for testing but provides an opportunity for design iteration prior to

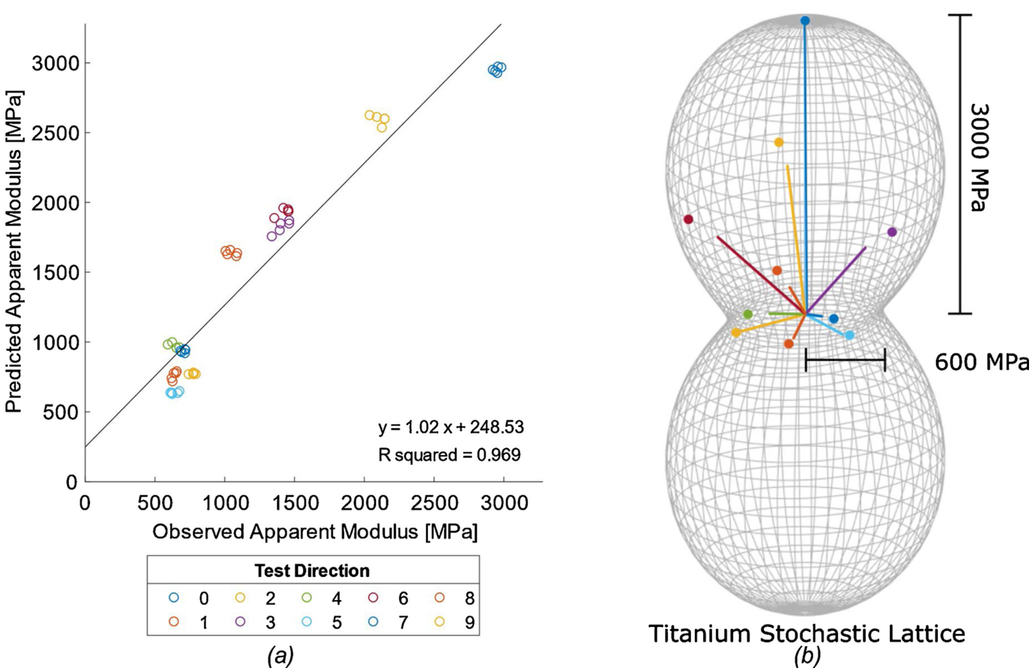

Fig. 4. (a) Predicted apparent modulus against their corresponding observed apparent modulus along each of the 10 tested vector directions for the purely predictive model for titanium stochastic structures. (b) Predicted anisotropic apparent modulus ellipsoid (grey), mean observed apparent modulus in each of the 10 directions (coloured lines) and predicted apparent modulus along those 10 directions (coloured dots). Legend applies to both figures and refers to the test directions in Table 1.

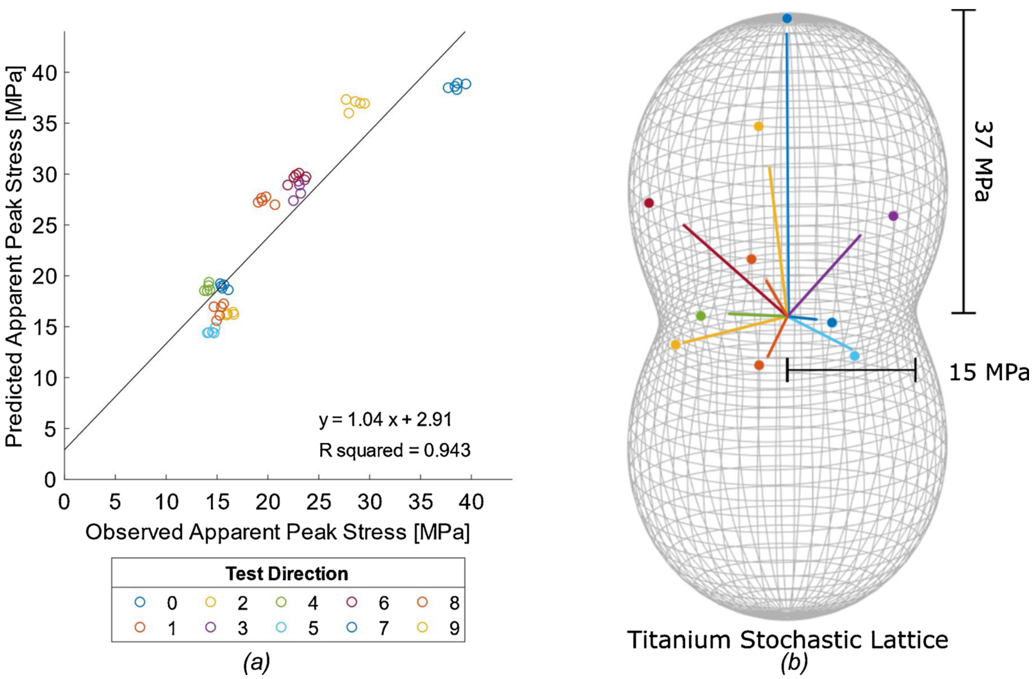

Fig. 5. (a) Predicted peak strength against the corresponding observed peak strength along each of the 10 tested vector directions for the purely predictive model for titanium stochastic structures. (b) Predicted anisotropic strength ellipsoid (grey), mean observed strength in each of the 10 directions (coloured lines) and predicted strength along those 10 directions (coloured dots). Legend applies to both figures and refers to the test directions in Table 1.

part manufacture which can reduce development time and costs. Our approach is an alternative method to finite element analysis for estimating off-axis modulus and strength but has the advantage that it doesn't need specialist and expensive software, no complex mesh is required, nor convergence problems are encountered. The stochastic structure used in our study was anisotropic with the highest apparent modulus of 2.9 GPa measured in the build direction and lowest apparent modulus of 0.6 – 0.8 GPa measured perpendicular to the build direction. The anisotropy was caused by the removal of low angle struts relative to the build direction, but it may be possible to generate more isotropic structures, for example by increasing the diameter of the lower angle struts or by decreasing the culling angle. The peak strength of this structure was highest in the build direction (40 MPa) and lowest in the direction perpendicular to the build direction (15 – 18 MPa).

The rhombic dodecahedron structure proved to be almost isotropic, with apparent modulus ranging from 110 MPa to 160 MPa and strength ranging from 4.1 MPa to 5.5 MPa. As for the stochastic specimens, for both apparent modulus and strength, the highest values were in the build direction and lowest values were perpendicular to the build direction. The nylon rhombic dodecahedron specimens had mechanical anisotropy of 1.5 for apparent modulus and 1.3 for strength.

Incorporation of lattice structures into load bearing components is possible, but consideration must be made for the different strength and failure mechanisms of lattice structures compared to the parent material. The proposed mathematical calculations provide a rapid way to assess strength in all loading axes at an early stage in component design, however, this method does not offer explanation of inherent mechanical deformation patterns and failure mechanisms under large deformation and the process could be supplemented with FE analysis to achieve this.

Previous methods for the prediction of mechanical properties have been based on either FEA or analytical methods, with all approaches focussing on repeating cells (Table 4).

Souza et al. reported an apparent modulus of between 0.01 and 14 GPa for steel repeating cell meshes, with a corresponding strength of 0.1–110 MPa [31]. Ferringo et al. predicted an apparent modulus between 76 – 111 GPa for Ti-6Al-4 V lattices. Both studies used models that overpredicted the apparent modulus and strength, within the same tolerance as the model presented in our paper. They attributed the overestimate to inaccurate modelling of shear properties and geometric imperfections in the printed specimens [31]. Few previous studies have validated models for mechanical properties of AM structures with mechanical testing or accounted for limitations of AM printing, instead studies have employed computational methods for repeating cells, less

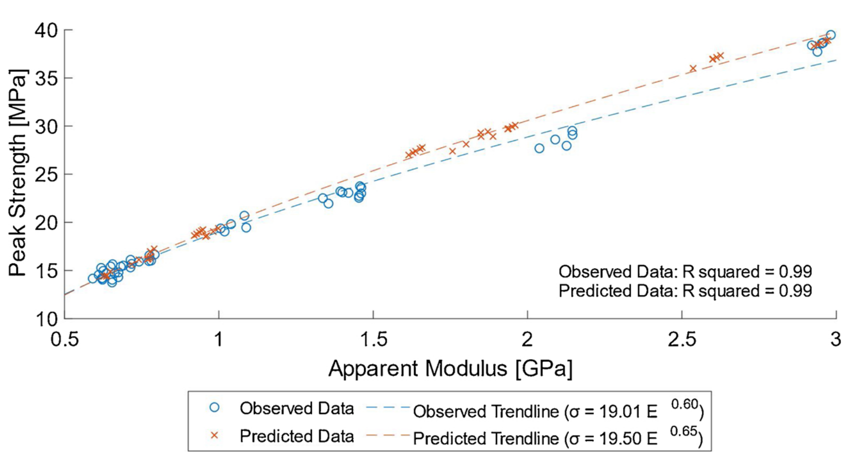

Fig. 6. Peak strength against apparent modulus for the observed and predicted data for the titanium stochastic specimens.

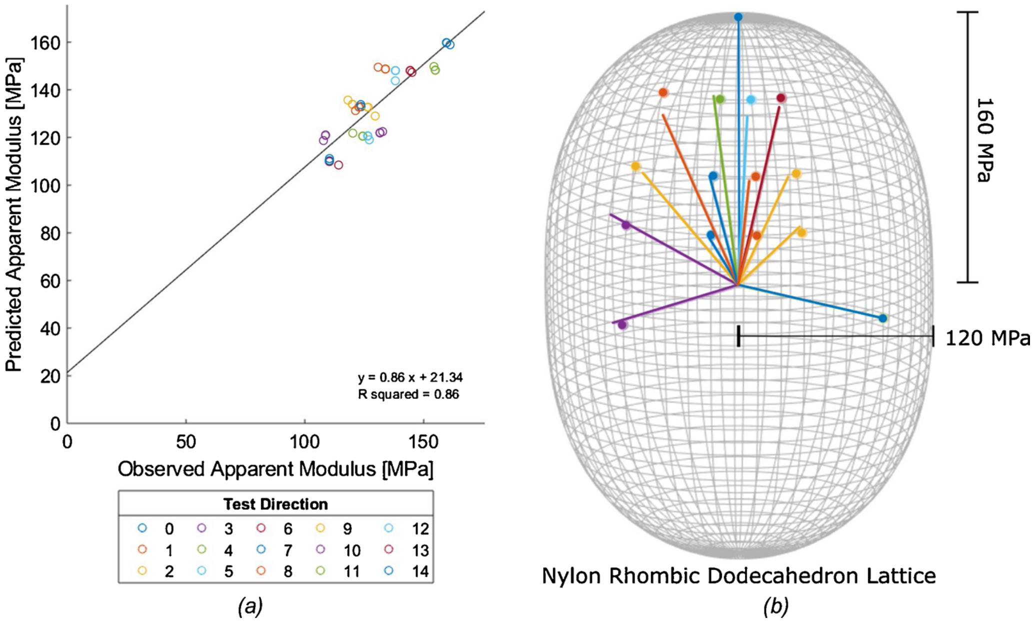

Fig. 7. (a) Predicted apparent modulus against their corresponding observed apparent modulus along each of the 10 tested vector directions for the purely predictive model for nylon rhombic dodecahedron structures. (b) Predicted anisotropic apparent modulus ellipsoid (grey), mean observed apparent modulus in each of the 15 directions (coloured lines) and predicted apparent modulus along those 15 directions (coloured dots). Legend applies to both figures and refers to the test directions in Table 1.

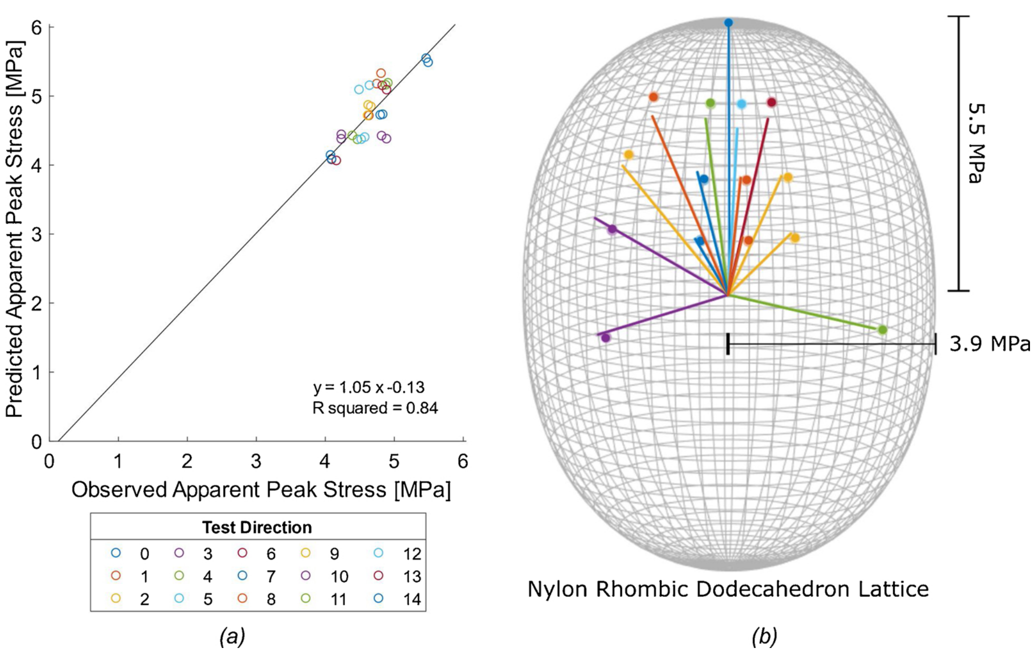

Fig. 8. (a) Predicted yield strength against the corresponding observed peak strength along each of the 10 tested vector directions for the purely predictive model for nylon rhombic dodecahedron structures. (b) Predicted anisotropic strength ellipsoid (grey), mean observed strength in each of the 15 directions (coloured lines) and predicted strength along those 15 directions (coloured dots). Legend applies to both figures and refers to the test directions in Table 1.

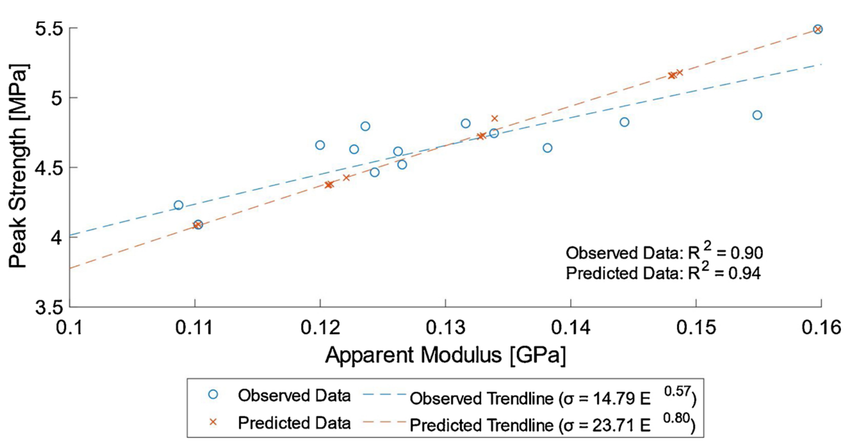

Fig. 9. Peak strength against apparent modulus for the observed and predicted data for nylon rhombic dodecahedron specimens.

Table 4
Summary of existing models for apparent modulus prediction in literature [31–33].

Author	Lattice Type	Material	Apparent Moduli	Strength [MPa]
Souza et al	8 BCC and FCC variants	Stainless steel 1.4404	0.01 – 14 GPa	0.1-110
McGregor et al	5 hexagonal variants	Thermoset polymers	0.4-610 MPa	0.04-34
Ferrigno et al	Octet and rhombic-dodecahedron	Ti-6Al-4V	76-111.3 GPa	281-955

suitable for stochastic structures, to validate their findings [31,34,35]. Although Souza et al. provide good data for structures designed with a range of apparent moduli and strengths suitable for use in bone implants, the presence of horizontal and low angle struts relative to the build direction complicates the reliable manufacture of the structures [31]. The results presented by McGregor et al. also demonstrate good prediction of properties over a suitable range, with mechanical validation, but the repeating unit hexagonal cell structures means hidden off-axis stiffness peaks will be present [32]. Ferrigno et al. provide another good model for apparent modulus and strength prediction with mechanical validation in one direction, however their range of apparent moduli and strengths lie outside of that required for the application of bone implants [33].

The relationships between predicted apparent modulus and strength across all test directions exhibited a power law trend for both structure types ($\sigma = 19.5\ E^{0.65}$ for stochastic specimens and $\sigma = 23.71\ E^{0.8}$ for rhombic dodecahedron specimens), as in Figs. 6 and 9. This relationship is similar for both the predicted and observed data. Furthermore, the presence of a power law between strength and apparent modulus is consistent with findings in literature where models with a range of coefficients and powers can be found [25,29,36].

Torsional stiffness and strength have been neglected when fitting the described model to the mechanical data. This limits this model to non-torsional analysis only, however, this has no detrimental effect on the results presented here as the orthotropic and torsional apparent modulus elements in the stiffness matrix are uncoupled. This method predicts static apparent modulus and strength whereas fatigue mechanical properties may be more suitable design considerations in some applications, particularly in bone implants [25]. We also tested at a fixed load rate which was less than physiological loading. However, previous studies have found relationships between dynamic and static mechanical properties which suggests that this model would be equally applicable to dynamic data. The method presented here requires an initial set of specimens to be manufactured and mechanically tested in orthogonal directions to determine apparent modulus and strength before any predictions of the mechanical properties of future structures can be tested. This is not necessary in FE methods, which can return structural mechanical data based on only material properties. Although it is time intensive, the use of mechanical data to form the models shown in this study means that the returned model has been calibrated and gave greater confidence in the model predictions. The variation in the model parameters explain the sensitivity in the fit. The over prediction and under prediction seen in the model results will have had a contribution from the model sensitivity. Calculating model fit parameters across the spread of experimental data suggests that k varies by 2.0%, l varies by 4.2% and λ varies by 4.9%. This sensitivity analysis indicates that other factors, such as the average density of off-axis specimens being 4.6% less than other specimens, led to the consistent over/under prediction as well. The effect of anisotropic microstructure of AM components is not accounted for in this model. Build orientation can cause a highly orientated microstructure resulting in inherent material anisotropy in AM components even if the geometry is isotropic such effects are not traditionally accounted for in FE methods. This is not explicitly accounted for in this model, however, the macroscale effects of localised material anisotropy are described by this model as observed mechanical data is used to define it. The macroscale effects of any microscale defects are accounted for in a similar way as strut defects can cause either random or systematic variation in mechanical properties. The method addresses random variations by fitting the models to mechanical properties for each measured sample, n = 5 for each test direction, and systematic variations by using observed mechanical data to define the model. Scanning electron microscope (SEM) images were also used to verify, across a small subpopulation of specimens, that no manufactured struts were misprinted or fractured. Variations in strut surfaces existed between the CAD data and the manufactured specimens, due to variations in the AM process, however, previous work demonstrated that the manufactured structures provided accurate realisation of the planned CAD data [25]. Differences in strut morphology were observed, between struts of different angles as well as top and bottom surfaces of lower angled struts, which may contribute to the errors observed.

The stochastic structures presented here have the potential to be used as a base lattice in the orthopaedic industry because their properties and anisotropy are similar to those of human bone. Both structures may also be useful for light-weight applications where a space-filling isotropic lattice with specific properties is required for load bearing or impact conditions. The deployment of such lattice structures requires a greater analysis of anisotropy than has historically been necessary for solid isotropic materials. Our method of predicting off axis stiffness and strength based on data from the orthogonal directions is a reliable and rapid way to assess these data and can be performed on CAD models which enables an early opportunity to control mechanical anisotropy.

5. Conclusion

Our model is the first to predict the anisotropic apparent modulus and strength of stochastic and rhombic dodecahedron structures based on lattice density and fabric tensors and will be highly useful in the mechanical design of lattice structures.

CRediT authorship contribution statement

Maxwell Munford: Conceptualization, Methodology, Software, Formal analysis, Writing - original draft, Visualization, Writing - review & editing. **Umar Hossain:** Investigation, Methodology, Resources, Data curation, Visualization, Writing - review & editing. **Shaaz Ghouse:** Supervision, Methodology, Writing - review & editing. **Jonathan R.T. Jeffers:** Supervision, Funding acquisition, Project administration, Writing - review & editing.

Acknowledgements

The authors wish to gratefully acknowledge the Engineering and Physical Sciences Research Council and Renishaw PLC for their financial and technical support of this study (EP/R042721/1, EP/K027549/1) and the Wellcome trust for their contributions via a translational partnership award (208858/Z/17/Z). The authors would also like to thank Natalie Reznikov for her contribution of the rhombic dodecahedron CAD data..

Appendix

The regression matrices for the known values of $\boldsymbol{y}$, the column vector containing the elements from the observed orthotropic compliance tensor, and $\boldsymbol{X}$ were formed as below for the system of equations ($\boldsymbol{y} = \boldsymbol{Xc} + \boldsymbol{e}$). Multiple data points for each row entry was performed so that a least squared regression could be performed to determine the coefficients in $\boldsymbol{c}$.

$$\begin{pmatrix} ln(\frac{1}{S_{11}}) \\ ln(\frac{1}{S_{22}}) \\ ln(\frac{1}{S_{33}}) \\ ln(\frac{\upsilon}{S_{11}}) \\ ln(\frac{\upsilon}{S_{22}}) \\ ln(\frac{\upsilon}{S_{33}}) \end{pmatrix} = \begin{pmatrix} 1 & 0 & 0 & 0 & 0 & 0 & ln(\frac{1}{\rho}) & ln(\frac{1}{{D_1}^2}) & 0 & 0 \\ 0 & 1 & 0 & 0 & 0 & 0 & ln(\frac{1}{\rho}) & 0 & ln(\frac{1}{{D_2}^2}) & 0 \\ 0 & 0 & 1 & 0 & 0 & 0 & ln(\frac{1}{\rho}) & 0 & 0 & ln(\frac{1}{{D_3}^2}) \\ 0 & 0 & 0 & 1 & 0 & 0 & ln(\frac{1}{\rho}) & ln(\frac{1}{D_1}) & ln(\frac{1}{D_2}) & 0 \\ 0 & 0 & 0 & 0 & 1 & 0 & ln(\frac{1}{\rho}) & ln(\frac{1}{D_1}) & 0 & ln(\frac{1}{D_3}) \\ 0 & 0 & 0 & 0 & 0 & 1 & ln(\frac{1}{\rho}) & 0 & ln(\frac{1}{D_2}) & ln(\frac{1}{D_3}) \end{pmatrix} \begin{pmatrix} ln(\lambda_{11}) \\ ln(\lambda_{22}) \\ ln(\lambda_{33}) \\ ln(\lambda_{12}) \\ ln(\lambda_{13}) \\ ln(\lambda_{23}) \\ k \\ l_1 \\ l_2 \\ l_3 \end{pmatrix} + \begin{pmatrix} e_1 \\ e_2 \\ e_3 \\ e_3 \\ e_4 \\ e_5 \\ e_6 \end{pmatrix}$$

Appendix B. Supplementary data

Supplementary material related to this article can be found, in the online version, at doi:https://doi.org/10.1016/j.addma.2020.101041.

References

[1] S. Tsopanos, R.A.W. Mines, S. McKown, Y. Shen, W.J. Cantwell, W. Brooks, C.J. Sutcliffe, The influence of processing parameters on the mechanical properties of selectively laser melted stainless steel microlattice structures, J. Manuf. Sci. Eng. 132 (4) (2010) 12, https://doi.org/10.1115/1.4001743 041011.

[2] Ł. Cyganik, M. Binkowski, G. Kokot, T. Rusin, P. Popik, F. Bolechała, R. Nowak, Z. Wróbel, A. John, Prediction of Young′s modulus of trabeculae in microscale using macro-scale′s relationships between bone density and mechanical properties, J. Mech. Behav. Biomed. Mater. 36 (2014) 120–134, https://doi.org/10.1016/J.JMBBM.2014.04.011.

[3] V.J. Challis, X. Xu, L.C. Zhang, A.P. Roberts, J.F. Grotowski, T.B. Sercombe, High specific strength and stiffness structures produced using selective laser melting, Mater. Des. 63 (2014) 783–788, https://doi.org/10.1016/j.matdes.2014.05.064.

[4] P. Zhang, J. Toman, Y. Yu, E. Biyikli, M. Kirca, M. Chmielus, A.C. To, Efficient design-optimization of variable-density hexagonal cellular structure by additive manufacturing: theory and validation, J. Manuf. Sci. Eng. (2015), https://doi.org/10.1115/1.4028724.

[5] N.R.B. Reznikov, S. Ghouse, A.E. Weston, U. Collinson, G.W. Blunn, J. Jeffers, J.P. Cobb, M.M. Stevens, Individual Response Variations in Scaffold-guided Bone Regeneration Are Determined by Independent Strain- and Injury-induced Mechanisms, (2018), https://doi.org/10.1074/jbc.RA118.003238.

[6] J. Martínez, J. Dumas, S. Lefebvre, Procedural voronoi foams for additive manufacturing, ACM Trans. Graph. 35 (4) (2016), https://doi.org/10.1145/2897824.2925922 Article no, 44.

[7] X. Wang, S. Xu, S. Zhou, W. Xu, M. Leary, P. Choong, M. Qian, M. Brandt, Y.M. Xie, Topological design and additive manufacturing of porous metals for bone scaffolds and orthopaedic implants: a review, Biomaterials. (2016), https://doi.org/10.1016/j.biomaterials.2016.01.012.

[8] V. Petrovic, J. Vicente, J. Ramn, L. Portols, Additive manufacturing solutions for improved medical implants, Biomedicine, (2012), https://doi.org/10.5772/38349.

[9] A. Hou, K. Gramoll, Design and fabrication of CFRP interstage attach fitting for launch vehicles, J. Aerosp. Eng. 12 (1999) 83–91, https://doi.org/10.1061/(ASCE)0893-1321(1999)12:3(83).

[10] S.K. Moon, Y.E. Tan, J. Hwang, Y.-J. Yoon, Application of 3D printing technology for designing light-weight unmanned aerial vehicle wing structures, Int. J. Precis. Eng. Manuf. Technol. 1 (2014) 223–228, https://doi.org/10.1007/s40684-014-0028-x.

[11] D.S. Elliott, K.J.H. Newman, D.P. Forward, D.M. Hahn, B. Ollivere, K. Kojima, R. Handley, N.D. Rossiter, J.J. Wixted, R.M. Smith, C.G. Moran, A unified theory of bone healing and nonunion BHN THEORY, (n.d.). doi:10.1302/0301-620X.98B7.

[12] A.L. Jardini, M.A. Larosa, C.A. de Carvalho Zavaglia, L.F. Bernardes, C.S. Lambert, P. Kharmandayan, D. Calderoni, R. Maciel Filho, Customised titanium implant fabricated in additive manufacturing for craniomaxillofacial surgery: this paper discusses the design and fabrication of a metallic implant for the reconstruction of a large cranial defect, Virtual Phys. Prototyp. 9 (2) (2014) 115–125, https://doi.org/10.1080/17452759.2014.900857.

[13] K.C. Wong, S.M. Kumta, K.H. Chiu, K.W. Cheung, K.S. Leung, P. Unwin, M.C.M. Wong, Computer assisted pelvic tumor resection and reconstruction with a custom-made prosthesis using an innovative adaptation and its validation, Comput. Aided Surg. 12 (4) (2007) 225–232, https://doi.org/10.1080/10929080701536046.

[14] C. Imediegwu, R. Murphy, R. Hewson, M. Santer, Multiscale structural optimization towards three-dimensional printable structures, Struct. Multidiscipl. Optim. (2019) 1–13, https://doi.org/10.1007/s00158-019-02220-y.

[15] V. Weißmann, R. Bader, H. Hansmann, N. Laufer, Influence of the structural orientation on the mechanical properties of selective laser melted Ti6Al4V open-porous scaffolds, Mater. Des. 95 (2016) 188–197, https://doi.org/10.1016/j.matdes.2016.01.095.

[16] E. Sallica-Leva, A.L. Jardini, J.B. Fogagnolo, Microstructure and mechanical behavior of porous Ti-6Al-4V parts obtained by selective laser melting, J. Mech. Behav. Biomed. Mater. 26 (2013) 98–108, https://doi.org/10.1016/j.jmbbm.2013.05.011.

[17] Y. Xu, D. Zhang, S. Hu, R. Chen, Y. Gu, X. Kong, J. Tao, Y. Jiang, Mechanical properties tailoring of topology optimized and selective laser melting fabricated Ti6Al4V lattice structure, J. Mech. Behav. Biomed. Mater. 99 (2019) 225–239, https://doi.org/10.1016/J.JMBBM.2019.06.021.

[18] T. Stanković, J. Mueller, K. Shea, The effect of anisotropy on the optimization of additively manufactured lattice structures, Addit. Manuf. 17 (2017) 67–76, https://doi.org/10.1016/J.ADDMA.2017.07.004.

[19] A. Takezawa, K. Yonekura, Y. Koizumi, X. Zhang, M. Kitamura, Isotropic Ti–6Al–4V lattice via topology optimization and electron-beam melting, Addit. Manuf. 22 (2018) 634–642, https://doi.org/10.1016/j.addma.2018.06.008.

[20] M. Tuncer, U.N. Hansen, A.A. Amis, Prediction of structural failure of tibial bone models under physiological loads: effect of CT density–modulus relationships, Med. Eng. Phys. 36 (2014) 991–997, https://doi.org/10.1016/J.MEDENGPHY.2014.04.006.

[21] S.M. Nazemi, M. Amini, S.A. Kontulainen, J.S. Milner, D.W. Holdsworth, B.A. Masri, D.R. Wilson, J.D. Johnston, Prediction of local proximal tibial subchondral bone structural stiffness using subject-specific finite element modeling: effect of selected density–modulus relationship, Clin. Biomech. Bristol Avon (Bristol, Avon) 30 (2015) 703–712, https://doi.org/10.1016/J.CLINBIOMECH.2015.05.002.

[22] P.K. Zysset, A review of morphology-elasticity relationships in human trabecular bone: theories and experiments, J. Biomech. 36 (2003) 1469–1485, https://doi.org/10.1016/S0021-9290(03)00128-3.

[23] J. Hazrati Marangalou, K. Ito, M. Cataldi, F. Taddei, B. van Rietbergen, A novel approach to estimate trabecular bone anisotropy using a database approach, J. Biomech. 46 (2013) 2356–2362, https://doi.org/10.1016/J.JBIOMECH.2013.07.042.

[24] S.C. Cowin, The relationship between the elasticity tensor and the fabric tensor, Mech. Mater. 4 (1985) 137–147, https://doi.org/10.1016/0167-6636(85)90012-2.

[25] S. Ghouse, S. Babu, K. Nai, P.A. Hooper, J.R.T. Jeffers, The influence of laser parameters, scanning strategies and material on the fatigue strength of a stochastic porous structure, Addit. Manuf. 22 (2018) 290–301, https://doi.org/10.1016/j.addma.2018.05.024.

[26] International Standard, ISO 13314 - Mechanical Testing of Metals, Ductility Testing, Compression Test for Porous and Cellular Metals, (2011).

[27] M. Moesen, L. Cardoso, S.C. Cowin, A symmetry invariant formulation of the relationship between the elasticity tensor and the fabric tensor, Mech. Mater. 54 (2012) 70–83, https://doi.org/10.1016/j.mechmat.2012.07.004.

[28] The MathWorks Inc., MATLAB, (2018).

[29] L.J. Gibson, The mechanical behaviour of cancellous bone, J. Biomech. 18 (5) (1985) 317–328, https://doi.org/10.1016/0021-9290(85)90287-8.

[30] I. Standard, INTERNATIONAL STANDARD Mechanical testing of metals — ductility testing — compression test for porous and cellular metals, Int. Stand. ISO 13314 (2011) doi: ISO 13314:2011.

[31] J. Souza, A. Großmann, C. Mittelstedt, Micromechanical analysis of the effective properties of lattice structures in additive manufacturing, Addit. Manuf. 23 (2018)

53–69, https://doi.org/10.1016/J.ADDMA.2018.07.007.
[32] D.J. McGregor, S. Tawfick, W.P. King, Mechanical properties of hexagonal lattice structures fabricated using continuous liquid interface production additive manufacturing, Addit. Manuf. 25 (2019) 10–18, https://doi.org/10.1016/J.ADDMA.2018.11.002.
[33] A. Ferrigno, F. Di Caprio, R. Borrelli, F. Auricchio, A. Vigliotti, The mechanical strength of Ti-6Al-4V columns with regular octet microstructure manufactured by electron beam melting, Materialia. 5 (2019) 100232, https://doi.org/10.1016/J.MTLA.2019.100232.
[34] S. Xu, J. Shen, S. Zhou, X. Huang, Y.M. Xie, Design of lattice structures with controlled anisotropy, Mater. Des. 93 (2016) 443–447, https://doi.org/10.1016/J.MATDES.2016.01.007.
[35] O. Rehme, Cellular design for laser freeform fabrication, schriftenreihe lasertechnik, Cuvillier Verlag 4 (2010), https://ebookcentral.proquest.com/lib/gbv/detail.action?docID=5020518.
[36] S. Ghouse, N. Reznikov, O.R. Boughton, S. Babu, K.C.G. Ng, G. Blunn, J.P. Cobb, M.M. Stevens, J.R.T. Jeffers, The design and in vivo testing of a locally stiffness-matched porous scaffold, Appl. Mater. Today 15 (2019) 377–388, https://doi.org/10.1016/J.APMT.2019.02.017.